Desiccation time during drought is highly predictable across species of Eucalyptus from contrasting climates

Christopher Blackman, Ximeng Li, Brenda Choat, Paul Rymer, Martin de Kauwe, Remko Duursma, David Tissue, Belinda Medlyn

HAL Id: hal-02278945
https://hal.science/hal-02278945

Submitted on 4 Sep 2019

Desiccation time during drought is highly predictable across species of *Eucalyptus* from contrasting climates

Chris J. Blackman[1,2] (iD), **Ximeng Li**[1] (iD), **Brendan Choat**[1] (iD), **Paul D. Rymer**[1] (iD), **Martin G. De Kauwe**[3] (iD), **Remko A. Duursma**[1] (iD), **David T. Tissue**[1] (iD) **and Belinda E. Medlyn**[1] (iD)

[1]Hawkesbury Institute for the Environment, Western Sydney University, Locked Bag 1797, Penrith, NSW 2751, Australia; [2]Université Clermont-Auvergne, INRA, PIAF, 63000, Clermont-Ferrand, France; [3]ARC Centre of Excellence for Extreme Climates, University of New South Wales, Sydney, NSW 2052, Australia

Summary

- Catastrophic failure of the water transport pathway in trees is a principal mechanism of mortality during extreme drought. To be able to predict the probability of mortality at an individual and landscape scale we need knowledge of the time for plants to reach critical levels of hydraulic failure.
- We grew plants of eight species of *Eucalyptus* originating from contrasting climates before allowing a subset to dehydrate. We tested whether a trait-based model of time to plant desiccation t_{crit}, from stomatal closure g_{s90} to a critical level of hydraulic dysfunction Ψ_{crit} is consistent with observed dry-down times.
- Plant desiccation time varied among species, ranging from 96.2 to 332 h at a vapour-pressure deficit of 1 kPa, and was highly predictable using the t_{crit} model in conjunction with a leaf shedding function. Plant desiccation time was longest in species with high cavitation resistance, strong vulnerability segmentation, wide stomatal-hydraulic safety, and a high ratio of total plant water content to leaf area.
- Knowledge of t_{crit} in combination with water-use traits that influence stomatal closure could significantly increase our ability to predict the timing of drought-induced mortality at tree and forest scales.

Introduction

Drought is a major environmental stress that strongly impacts forest productivity and growth, and under extreme conditions can cause tree death and lead to a shift in community species composition (Nepstad *et al.*, 2007). Recent reports of drought-induced tree mortality in a wide range of forests (Nardini *et al.*, 2013; Moore *et al.*, 2016; Venturas *et al.*, 2016; Duke *et al.*, 2017), combined with predictions of more extreme drought occurring with global warming (Trenberth *et al.*, 2014), has focused research attention on the mechanisms of tree mortality. This work indicates that a major cause of drought mortality is catastrophic failure of the plant water transport (hydraulic) system (Brodribb & Cochard, 2009; Anderegg *et al.*, 2015; Adams *et al.*, 2017; Choat *et al.*, 2018). However, despite these efforts, we still find it challenging to predict when lethal thresholds of water stress will be reached during drought. One major obstacle to such predictions is that we still have only limited knowledge of the plant traits that determine plant desiccation times to hydraulic failure.

During drought, plants typically close their stomata as a first response to minimize water loss (Martin-StPaul *et al.*, 2017; Li *et al.*, 2018a). However, if drought persists, tension within the water-conducting xylem will increase as plants dehydrate via water loss through permeable leaf cuticles and leaky stomata (Kerstiens, 1996; Brodribb *et al.*, 2014; Schuster *et al.*, 2017; Duursma *et al.*, 2019). Without relief, increasing xylem tension can cause cavitation and widespread embolism (air bubbles that block water transport), leading to hydraulic dysfunction and plant death (Tyree & Sperry, 1989). The ability of plants to resist drought-induced cavitation is expressed in terms of their hydraulic vulnerability and measured as the xylem water potential Ψ_x (megapascal) corresponding to a percentage loss of hydraulic conductivity due to embolism. Previous work has shown a strong correspondence between drought mortality and 50% loss of stem conductivity in conifers (Brodribb & Cochard, 2009) and 88–95% loss of stem conductivity in angiosperms (Resco *et al.*, 2009; Urli *et al.*, 2013; Li *et al.*, 2016). Quantifying hydraulic vulnerability, as well as the safety margin between the point of stomatal closure and critical thresholds of hydraulic failure (Delzon & Cochard, 2014; Skelton *et al.*, 2015; Martin-StPaul *et al.*, 2017), is key to understanding species mortality risk under future drought scenarios (Brodribb, 2009; Choat *et al.*, 2012, 2018; Anderegg *et al.*, 2016). Nevertheless, these traits are largely static and do not provide information about when plants will reach critical thresholds of hydraulic failure, limiting our predictive capacity.

To help address this question of the timing of hydraulic failure, additional traits that influence the dynamics of plant

dehydration, including hydraulic capacitance, minimum leaf conductance, and plant allometry, have recently been integrated into models of plant desiccation time (Blackman *et al.*, 2016; Martin-StPaul *et al.*, 2017). Plant hydraulic capacitance describes the extent to which internal compartments of water stored in leaves, stems, and roots buffer decreases in xylem water potential during drought (Pineda-Garcia *et al.*, 2013; Salomon *et al.*, 2017). By definition, plants with high hydraulic capacitance lose more water per decrease in Ψ_x than plants with low capacitance. They often exhibit large internal water storage reservoirs and are typically described in terms of their desiccation avoidance strategy. However, functional trade-offs between hydraulic capacitance and cavitation resistance mean plants with high capacitance tend to be relatively vulnerable to cavitation (Scholz *et al.*, 2011) and not necessarily less susceptible to drought mortality.

The dynamics of plant desiccation during drought are also dependent on canopy-level processes, such as the minimum rate of water loss from leaves g_{min}. Because g_{min} sets the rate of water loss from leaves following stomatal closure, it should at least theoretically have a strong influence on the time dependence of hydraulic failure (Blackman *et al.*, 2016; Martin-StPaul *et al.*, 2017). Ultimately, g_{min} is meaningful for understanding rates of whole plant desiccation when it is normalized by canopy leaf area. However, canopy leaf area is rarely constant during drought, with leaf shedding known as a key water-saving mechanism (Bucci *et al.*, 2005).

Taken together, quantifying these traits and processes will increase our ability to determine how long it takes plants to deplete internal water storage pools and reach critical levels of drought stress; yet, their individual and combined influence on the timing of hydraulic failure remains untested experimentally. Here, we measured the dynamics of plant desiccation in 1–2 m tall plants grown under common conditions during a dry-down experiment and compared the results with output from a trait-based model of the time t_{crit} (expressed in vapour-pressure deficit multiplied by hours, VPD-h) it takes plants to desiccate from the point of stomatal closure to critical levels of water stress (Blackman *et al.*, 2016). The model derived t_{crit} is described as follows:

$$t_{crit} = \frac{(\theta_0 - C\psi_{crit})V_w}{L_m g_{min} D} \qquad \text{Eqn 1}$$

where θ_0, total plant relative water content (RWC, g g^{-1}) at stomatal closure (taken to be 90% reduction in g_s, or g_{s90}); $C\Psi_{crit}$, combined term that is a function of Ψ_{crit} (in this study with angiosperms, we used the water potential at 88% loss of stem conductivity) and shoot capacitance C (the slope of RWC vs Ψ) and represents the RWC at Ψ_{crit} (i.e. θ_{crit}); V_w, maximum total amount of water in the plant (g); L_m, maximum total leaf area (m^2); g_{min}, the minimum leaf conductance (g m^{-2} s^{-1}); D, VPD (mol mol^{-1})).

We parameterized the model using traits derived from leaves, shoots, and whole plants, and incorporated a leaf shedding function based on changes in leaf area in response to drought. Comparisons between observed and predicted desiccation time were

made across eight species of *Eucalyptus* representing vegetation types from tall wet forest to semi-arid woodland in eastern and central Australia. In addition to their importance to Australian ecosystems, eucalypts are economically important as forest trees around the world (Booth *et al.*, 2015). Recent reports of drought-induced dieback and mortality of eucalypt trees (Matusick *et al.*, 2013; Li *et al.*, 2018b) suggest eucalypt-dominated forests may be susceptible to global-change-type drought. In accordance with the model, we hypothesized that plants (species) with longer dry-down times would exhibit the following characteristics: greater breadth in the span of RWC between the point of stomatal closure and critical levels of hydraulic failure; leaves with lower minimum conductance; and higher ratio of total plant water content to canopy leaf area. However, considering that trade-offs exist between traits that affect some of these characteristics, such as cavitation resistance and water-holding capacity, it is unlikely for species to maximize all traits simultaneously.

Materials and Methods

Species

Eight species of *Eucalyptus* were chosen to test whether plant desiccation times are predictable using the t_{crit} model. These species represent a wide range of drought tolerances (Li *et al.*, 2018a) that were predicted to generate a wide range of desiccation times. The eight species are dominant forest trees, representing four major vegetation types within southeastern and central Australia (Table 1). Climatic conditions calculated across each species distribution vary widely, with mean annual precipitation (MAP)

Table 1 Summary of species names and identification, vegetation type (VT), and home-climate variables mean annual precipitation (MAP), mean annual temperature (MAT), aridity index (AI), mean annual vapour-pressure deficit (D_{ave}), and maximum mean monthly vapour pressure deficit (D_{max}).

Species (spp.)	VT	MAP (mm)	MAT (°C)	AI	D_{ave} (kPa)	D_{max} (kPa)
Eucalyptus grandis	WSF	1436.3	18.5	1.08	0.23	0.53
Eucalyptus viminalis	WSF	803.3	13.2	1.0	0.18	0.62
Eucalyptus blakelyi	GW	717.6	14.9	0.65	0.31	0.94
Eucalyptus machroryncha	GW	736.3	13.7	0.86	0.26	0.86
Eucalyptus melliodora	GW	677.7	14.5	0.67	0.29	0.88
Eucalyptus sideroxylon	DSF	641.9	16.3	0.53	0.41	1.11
Eucalyptus largiflorens	SAW	333.3	17.5	0.26	0.55	1.43
Eucalyptus populnea	SAW	498.1	18.8	0.29	0.65	1.49

WSF, wet sclerophyll forest; GW, grassy woodland; DSF, dry sclerophyll forest; SAW, semi-arid woodland. Climate variables were downloaded from the Atlas of Living Australia website at http://www.ala.org.au.

ranging from 333 to 1436 mm and mean annual temperature ranging from 13.2 to 18.8°C (Table 1).

Experimental design

Plants from eight *Eucalyptus* species were grown under well-watered, common garden conditions inside a polytunnel growth facility (Richmond, NSW, Australia). Seed was sourced from the Australian Tree Seed Centre in May 2017 and germinated at Greening Australia's production nursery located in Richmond, NSW Australia. On 21 September 2017, following roughly 4 months of growth, 15–20 seedlings per species were moved to a polytunnel growth facility located at the Hawkesbury campus of Western Sydney University (Richmond, NSW, Australia) and transplanted into 25 l woven bags filled with a native loamy sand top-soil (Menangle, NSW, Australia), supplemented with slow-release fertilizer. Bags were placed onto pallets to avoid root contact with the soil. Planting layout followed a split-block design, with three to four plants per species randomly positioned within each block. A single row of border plants consisted of randomly selected species. Plants were irrigated every second day to ensure soil water content remained at field capacity. A weather station consisting of a data-logger (CR300; Campbell Scientific Inc., Logan, UT, USA) connected to a light sensor (Decagon Devices Inc., Pullman, WA, USA), and temperature/relative humidity probe (HMP60-L; Campbell Scientific Inc.) was installed at 1.5 m above the ground and recorded temperature (°C) and relative humidity every 5 min throughout the experiment. During the experimental period, mean daily photon flux density was 6.67 mol, mean daily temperature was 22.6°C, and mean daily relative humidity was 64.3%.

In March 2018, after *c.* 7 months of growth under well-watered conditions, plants of each species were separated into three subgroups based on whether they showed relatively fast (group 1, consisting of *Eucalyptus blakleyi*, *Eucalyptus grandis*, and *Eucalyptus viminalis*), moderate (group 2, consisting of *Eucalyptus melliodora* and *Eucalyptus sideroxylon*), or slow (group 3, consisting of *Eucalyptus largiflorens*, *Eucalyptus macrorhyncha*, and *Eucalyptus populnea*) growth. We subsequently staggered the commencement of plant dry-down across the three groups, with plants from group 1 commencing in early March, group 2 in late March, and group 3 in early April. This process helped ensure plants were relatively uniform in size across species and large enough to minimize the effect of leaf sampling on plant dry-down times. At the start of each dry-down experiment, average plant height was 141 cm, 106 cm, and 160 cm for *E. blakleyi*, *E. grandis*, and *E. viminalis*, respectively; 144 cm and 154 cm for *E. melliodora* and *E. sideroxylon*, respectively; and 132 cm, 172 cm, and 100 cm for *E. largiflorens*, *E. macrorhyncha*, and *E. populnea*, respectively.

All plants were drought hardened by withholding water until early signs of leaf wilt were present, after which they were rewatered and allowed to recover for 4–6 d. This process was designed to increase species drought tolerance (Bartlett *et al.*, 2014) and reduce the likelihood that plants would suffer from drought 'shock' during the early stages of dehydration. At the end of this recovery period, between four and six plants per species were designated for a range of trait measurements, including specific leaf area, saturated water content, leaf pressure–volume analysis, shoot capacitance, minimum leaf conductance, and leaf hydraulic vulnerability. Water was withheld from the remaining plants per species ($n = 5$–12), after which they were allowed to deplete available soil water and dehydrate.

Plant water status of each individual was monitored regularly during the dry-down phase by measuring the water potential Ψ using a Scholander-type pressure chamber (PMS, Corvallis, OR, USA) on a mid–upper canopy leaf at predawn. Beyond the point of stomatal closure, the predawn water potential was always lower than the midday water potential that was occasionally measured the previous day (data not shown) and thus represents the maximum level of drought stress at that time during the final dry-down phase. After each Ψ measurement, the leaf was weighed for fresh mass and then oven-dried for leaf dry mass determination. Importantly, leaf sampling for water potential measurements had minimal impact ($< 5\%$) on total canopy leaf area. Each individual was also checked daily for signs of leaf death, which tended to occur first in older leaves near the base of the stem. Leaves were deemed to be dead (i.e. desiccated) when they became pale in colour and 'crispy' to touch. Dead leaves were collected and oven-dried. Cumulative leaf death was expressed on an area basis by multiplying leaf dry mass (grams) by species mean specific leaf area (SLA). When individual plants of each species reached predawn water potentials at or beyond Ψ_{crit}, the remaining aboveground shoot component was excised at soil level for harvesting. At these water potentials, plants typically exhibited a *c.* 50–75% reduction in canopy area due to leaf death. The roots were later separated from the soil via washing in water. All plant material was placed inside paper bags and oven-dried.

Stomatal closure

The stomatal closure point was determined for each species as the water potential associated with a 90% reduction in stomatal conductance from maximum mean values measured under pre-stress conditions (g_{s90}; see Supporting Information Table S1). The values were sourced from a previous study using plants of the same species grown and dried-down under approximately the same environmental conditions (Li *et al.*, 2018a).

Hydraulic vulnerability

Leaf hydraulic vulnerability to drought-induced embolism was determined for each species using the optical visualization technique (Brodribb *et al.*, 2016) on drought-hardened plant material grown in the current experiment ($n = 3$ per species). These data and species vulnerability curves are available in a separate publication (Li *et al.*, 2019; see Table S1).

Stem hydraulic vulnerability to drought-induced embolism was characterized for each species in a previous study (Li *et al.*, 2018a) using the bench dehydration technique on plant material grown under approximately the same

environmental conditions. The critical level of hydraulic dysfunction Ψ_{crit} in stems was defined as the water potential associated with an 88% reduction in stem hydraulic conductivity (see Table S1).

Shoot capacitance curves

The relationship between plant water potential and RWC was determined by drying-down shoots from full hydration to water potentials equal to or below Ψ_{crit}. The entire aboveground shoots of three plants per species ($n = 3$) were excised at predawn and immediately placed in large plastic bags and transported to the laboratory. At this time, plant water potential was > -0.1 MPa for all species. Two leaves per shoot were excised and placed in a Scholander-type pressure chamber for water potential determination. In all cases, shoots were well hydrated (water potential > -0.1 MPa). The shoot was then weighed on an open-top 0.01 g balance (MS3002S; Mettler Toledo, Columbus, OH, USA) and allowed to dehydrate on the bench over the course of 3–6 d, during which time water potential and shoot mass were measured repeatedly. Before each measurement, shoots were placed inside large plastic bags for c. 1 h to aid water potential equilibration. Nevertheless, it was assumed that leaf and stem water potential were in close equilibrium beyond the stomatal closure point. At the end of the dry-down experiment, leaves and stems were oven-dried and weighed for total dry mass determination. For species trait comparisons, a measure of the post leaf turgor loss shoot capacitance (mol kg^{-1} MPa^{-1}) was calculated for each species by dividing the linear portion of the post turgor loss RWC vs Ψ relationship by total maximum water content and dry mass (Table S1).

SLA and saturated water content

Before the commencement of the shoot capacitance measurements, a sample of 10–15 representative canopy leaves were excised from each shoot, weighed and scanned for leaf area determination and then oven-dried for 60 h. SLA (m^2 kg^{-1}) was calculated as projected leaf area divided by leaf dry mass (for species mean SLA values, see Table S1), and the leaf saturated water content (g g^{-1}) was calculated as (leaf saturated mass − leaf dry mass)/leaf dry mass. The saturated water content (g g^{-1}) of the three shoots per species was calculated as (shoot hydrated mass − shoot dry mass)/shoot dry mass. Meanwhile, a small 3–5 cm section of root was excised from the same plants per species and submersed in water for 2 h. Fully hydrated root sections were then blotted dry with a paper towel and weighed for saturated mass and then oven-dried and weighed for dry mass. The saturated water content of roots (g g^{-1}) was calculated as (root saturated mass − root dry mass)/root dry mass.

Pressure–volume curves

Two leaves from each of three randomly selected drought-hardened individuals per species were sampled and measured using

standard procedure (Tyree & Hammel, 1972). For each leaf, turgor loss point (Table S1) was determined from the beginning of the linear phase of the inverse water potential vs relative water content relationship.

Minimum leaf conductance

The minimum leaf conductance g_{min} was calculated from two detached leaves from each of three randomly selected drought-hardened individuals per species. Each leaf was scanned for leaf area, weighed using a precision balance, and the cut petiole sealed with wax before being pegged to a line of string suspended inside a climate-controlled growth chamber. The temperature and relative humidity inside the chamber were set to 20°C and 70%, respectively. Leaves were dried for a period of 7–10 h under low light conditions (200 µmol m^{-2} s^{-1}), with inbuilt fans blowing air across the leaf surface. During this time, leaves were weighed approximately every hour. Minimum conductance was calculated from the slope of the linear part of the leaf mass vs time relationship and converted to units of mmol m^{-2} s^{-1} in conjunction with chamber VPD (mol mol^{-1}) and double-sided leaf area.

Observed plant desiccation time

The time at which plants of each species dehydrated to water potentials at stomatal closure g_{s90} and Ψ_{crit} was interpolated from the relationship between predawn water potential and time (hours) multiplied by the average VPD measured over the course of the dry-down phase for each individual (see Fig. 1). The average time (VPD-h) between the water potential at g_{s90} and Ψ_{crit} was determined for each species from a linear mixed model (with individual input as a random factor) fitted to the Ψ–VPD-h data across individuals ($n = 5$–12). The resultant plant desiccation time (VPD-h, mol mol^{-1} h) observed for plants of each species is referred to as t_{crit_obs}.

The t_{crit} model

Predicted plant desiccation time was calculated for each individual used in the dry-down experiment. For model parameterization (see Eqn 1), species mean values were used for the relative water content at stomatal closure θ_0, the relative water content at Ψ_{crit} θ_{crit}, and the minimum leaf conductance g_{min}. Both θ_0 and θ_{crit} were calculated from the relationship between RWC and MPa derived from each species' shoot capacitance curve. For each species there was a marked phase at very low water potentials where the slope of the RWC vs Ψ relationship became shallower (Fig. S1). This is consistent with previous findings and suggests residual water is held tightly within parts the xylem matrix at very low water potentials (Tyree & Yang, 1990). Thus, for model parameterization, an exponential function fitted to the post turgor loss RWC vs Ψ relationship (using pooled data from three shoots per species) was used to determine θ_0 and θ_{crit}, the RWCs at g_{s90} and Ψ_{crit}, respectively. Importantly, it was assumed that the shoot RWC vs Ψ relationship was the same when measured in branches in the laboratory and potted plants during dehydration.
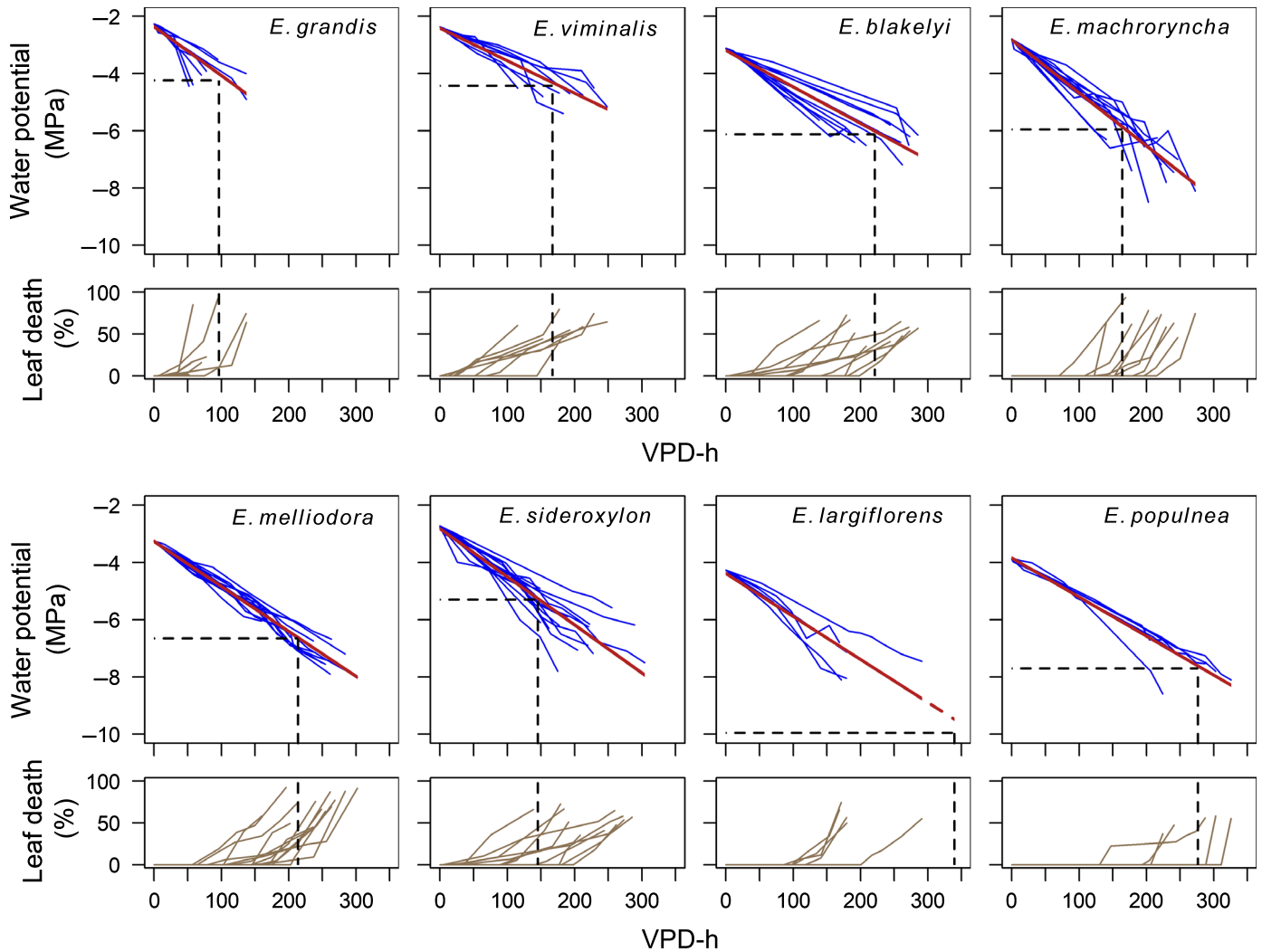
Fig. 1 The observed response of predawn water potential (MPa; large panels) and cumulative leaf death (expressed as percentage of total leaf area; small panels) for individuals of each *Eucalyptus* species over time (hours) adjusted for vapour-pressure deficit (VPD-h, mol mol^{-1} h) during dehydration from stomatal closure to when plants were harvested (*c*. 50–70% leaf death). The regression line (red) was determined for each species by fitting a mixed-effects model. This function was used to determine the accumulated VPD-hours (vertical dashed line) at Ψ_{crit} (horizontal dashed line). Panels are ordered for species home-site climate from wettest (upper left) to driest (lower right).

Meanwhile, the maximum total amount of water V_w was calculated for each individual by multiplying shoot plus root dry mass by species mean shoot and root saturated water content, respectively. The total leaf area L_m was calculated for each individual by multiplying total leaf dry mass by species mean SLA. The VPD D (mol mol^{-1}) was calculated as the average D experienced by each individual from stomatal closure to Ψ_{crit}. See Table 2 for model parameters for each species.

The t_{crit} model was parameterized in three ways: first, using the aforementioned traits with V_w derived from shoots only and with fixed leaf area; second, using the aforementioned traits with V_w including the contribution of roots and with fixed leaf area; and third, using whole-plant traits but with an added leaf shedding function. These three different approaches are referred to as t_{crit_shoot}, t_{crit}, and t_{crit_shed}, respectively.

Leaf shedding L was modelled as a two-stage process during drought, whereby total canopy leaf area is maximal up to the onset of leaf shedding and then declines linearly as cumulative leaf death increases with continued decreasing RWC. Segmented regression was fitted to species data pooled by vegetation type of cumulative leaf death vs leaf RWC (Fig. S2; Table S2). We constrained the data by vegetation type on the basis that fits by individual species gave unrealistic parameters, possibly because the leaf shedding data were not very precise for some species. Importantly, we could use leaf RWC data to fit the segmented regression and apply it to the model on the basis of strong correspondence between the RWC vs Ψ relationships derived from leaf and the shoot level pressure–volume curves, as well as from leaves sampled from potted plants during dehydration (Fig. S3).

Integrated with the t_{crit} model (see Notes S1 for full model derivation), the combined time below and above the leaf shedding break point was calculated as follows:

Comment citer ce document :
Blackman, C., Li, X., Choat, B., Rymer, P., De Kauwe, M., Duursma, R., Tissue, D., Medlyn, B. (2019). Desiccation time during drought is highly predictable across species of Eucalyptus from contrasting climates. New Phytologist, 12. , DOI : 10.1111/nph.16042

Table 2 Species trait means (± SE where appropriate) derived from leaves, shoots, and whole plants and used to calculate the time (without adjustment in leaf area) from stomatal closure to Ψ_{crit}.

Species	θ_0 (RWC)	θ_{crit} (RWC)	V_W (g)	L_m (m²)	g_{min} (mmol m⁻² s⁻¹)	D (mol mol⁻¹)
Eucalyptus grandis	0.69	0.43	202.1 ± 12.6	0.76 ± 0.05	1.59 ± 0.09	0.91 ± 0.02
Eucalyptus viminalis	0.66	0.34	203.6 ± 15.5	0.77 ± 0.06	0.96 ± 0.07	1.16 ± 0.05
Eucalyptus blakelyi	0.62	0.31	178.2 ± 14.7	0.55 ± 0.04	0.86 ± 0.10	1.16 ± 0.05
Eucalyptus machroryncha	0.74	0.37	198.9 ± 14.0	0.52 ± 0.04	2.03 ± 0.21	0.93 ± 0.01
Eucalyptus melliodora	0.58	0.26	139.0 ± 7.1	0.44 ± 0.03	1.07 ± 0.16	1.17 ± 0.04
Eucalyptus sideroxylon	0.65	0.35	155.1 ± 15.4	0.39 ± 0.04	1.47 ± 0.07	1.10 ± 0.03
Eucalyptus largiflorens	0.64	0.28	89.0 ± 9.4	0.17 ± 0.02	1.78 ± 0.09	0.78 ± 0.03
Eucalyptus populnea	0.75	0.45	95.1 ± 8.4	0.23 ± 0.02	1.40 ± 0.06	0.71 ± 0.05

See the Materials and Methods section for details of replication for specific traits. θ_0, branch relative water content (RWC) at stomatal closure ($g_s P_{90}$); θ_{crit}, branch RWC at 88% loss of stem hydraulic conductivity; V_w, total plant water content; L_m, total canopy leaf area; g_{min}, minimum leaf conductance; D, vapour pressure deficit during plant dry-down.

$$t_{crit\_shed} = \frac{b\theta_0 - (1-a) - \log_e(bC\psi_{crit} + a)}{bL_m g_{min} D} V_W \qquad \text{Eqn 2}$$

where θ_0, RWC at stomatal closure; $C\Psi_{crit}$, combined term that is a function of Ψ_{crit} (the water potential at 88% loss of stem conductivity) and shoot capacitance C (the slope of RWC vs Ψ) and represents the RWC at Ψ_{crit} (i.e. θ_{crit}); L_m, maximum total leaf area (m²); g_{min}, minimum leaf conductance (g m⁻² s⁻¹); V_w, total plant water content; D, VPD (mol mol⁻¹); a, intercept of post-cumulative leaf death vs leaf RWC relationship; b, slope of post-cumulative leaf death vs leaf RWC relationship.

Additional statistics

Linear regression analysis was used to test for significant bivariate relationships between predicted and observed plant desiccation time, between t_{crit_obs} and individual components of t_{crit}, and between t_{crit_obs} and key hydraulic traits. All analyses were performed in R v.3.5.2 (R Core Team, 2018).

Results

Observed vs predicted dry-down times

The actual time (hours) for plants to desiccate from the point of stomatal closure to critical levels of hydraulic dysfunction varied across species, ranging from 105.8 h (4.4 d) in the wet sclerophyll forest species *E. grandis*, to 425.6 h (17.7 d) in the semi-arid woodland species *E. largiflorens*. Once standardized by VPD (VPD-h, mol mol⁻¹ h), the observed time t_{crit_obs} varied across species, ranging from 96.3 VPD-h (*c.* 4 VPD-d) in *E. grandis*, to 332 VPD-h (*c.* 14 VPD-d) in *E. largiflorens* (Fig. 1; Table 3). Leaf shedding was observed in plants of all species during drought (Fig. 1), but the onset and progression of leaf shedding in response to decreasing water potential (megapascals) varied strongly among species, in accordance with their ecological niche (Fig. S4).

A very strong relationship was found across species between modelled and observed (t_{crit_obs}) plant desiccation time (Fig. 2).

Nevertheless, both t_{crit_shoot} and t_{crit} underestimated t_{crit_obs} across species, with increasing underestimation in species with longer t_{crit_obs} (Fig. 2a,b). When the model was extended to incorporate a leaf shedding function (t_{crit_shed}), estimated plant desiccation time increased for each species, albeit to varying degrees. The magnitude of this increase (relative to t_{crit}) ranged from 7.7 VPD-h (*c.* 0.3 VPD-d) in *E. macroryncha* to a much larger 126.5 VPD-h (*c.* 5 VPD-d) in *E. largiflorens* (Table 3). Strong correspondence to the 1 : 1 line was observed across species between t_{crit_obs} and t_{crit_shed} ($r^2 = 0.89$; intercept, −19.6; slope, 0.97; Fig. 2c). There was no cross-species relationship between predicted and observed desiccation times when t_{crit} was calculated using the VPD measured across each species' native distribution, whether it was the mean annual VPD ($r^2 = 0.04$) or the maximum mean monthly VPD ($r^2 = 0.03$) (Fig. S5).

Correlations with t_{crit_obs}

Across species, observed plant desiccation time t_{crit_obs} was negatively correlated both with mean maximum total water content

Table 3 Species values ($n = 5$–12) for the actual time (in hours, h) and observed (t_{crit_obs}) and predicted desiccation times normalised by vapour pressure deficit (VPD-h, mol mol⁻¹ h) from stomatal closure to Ψ_{crit}.

Species	Time (h)	t_{crit_obs} (VPD-h)	t_{crit} (VPD-h)	t_{crit_shed} (VPD-h)	t_{crit_shoot} (VPD-h)
Eucalyptus grandis	105.8	96.3	73.7	88.3	50.2
Eucalyptus viminalis	143.9	166.9	120.8	166.5	106.8
Eucalyptus blakelyi	190.6	221.1	159.4	183.9	143.7
Eucalyptus machroryncha	176.1	163.8	115.7	123.4	84.5
Eucalyptus melliodora	182.6	213.6	129.3	163.4	126.4
Eucalyptus sideroxylon	132.0	145.2	115.4	127.6	88.8
Eucalyptus largiflorens	425.6	332.0	215.6	342.1	149.3
Eucalyptus populnea	388.9	276.1	192.8	213.9	152.6

The various predicted dry-down times were calculated from (1) whole plant-level traits with fixed leaf area (t_{crit}), (2) whole plant-level traits with leaf shedding (t_{crit_shed}), and (3) shoot-level traits with fixed leaf area and $D = 1$ kPa (t_{crit_shoot}).

Version postprint
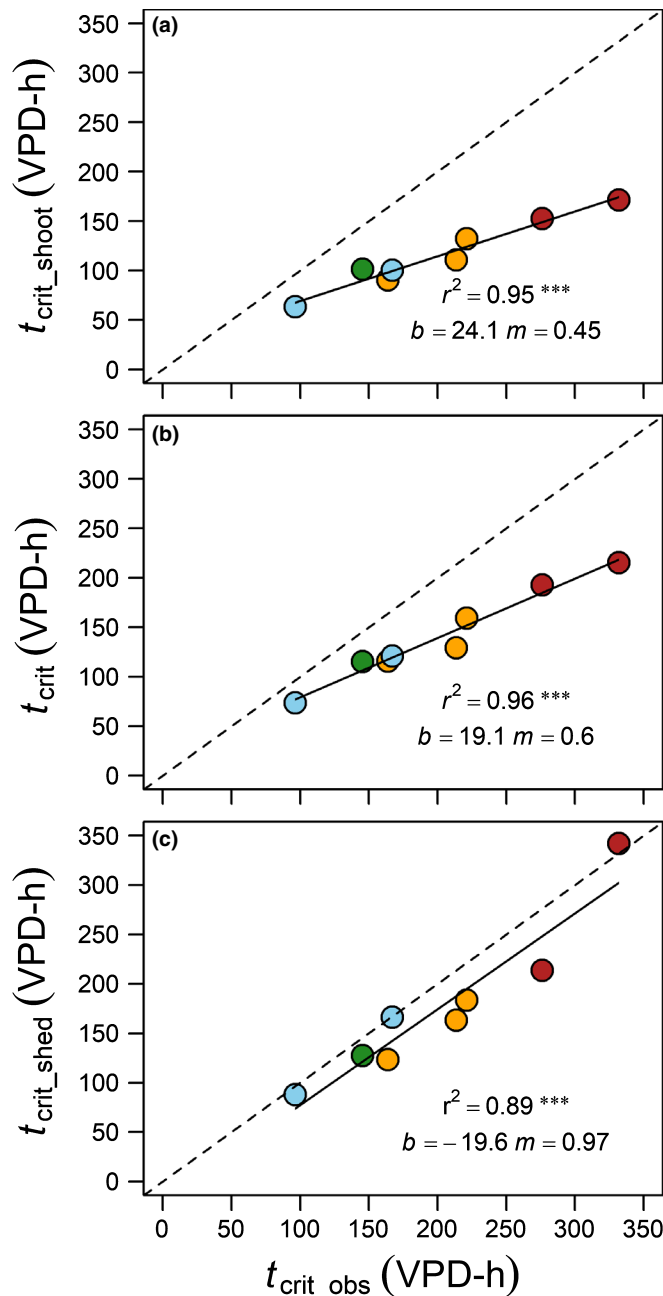
Fig. 2 Observed (t_{crit_obs}) vs modelled desiccation times (VPD-h, mol mol^{-1} h) for each *Eucalyptus* species. Modelled plant desiccation times were calculated using (a) shoot-level traits t_{crit_shoot}, (b) whole plant traits (including roots) with a fixed leaf area t_{crit}, and (c) whole plant traits combined with leaf shedding t_{crit_shed}. Colours indicate vegetation type: light blue, wet sclerophyll forest; green, dry sclerophyll forest; orange, grassy woodland; red, semi-arid woodland. In each panel, the slope m and intercept b are indicated. Levels of significance: ***, $P < 0.001$.

V_w ($r^2 = 0.73$, $P < 0.01$; Fig. 3d) and maximum leaf area L_m ($r^2 = 0.66$, $P < 0.05$; Fig. 3e). Nevertheless, t_{crit_obs} was positively correlated with the mean ratio of V_w to L_m across species ($r^2 = 0.5$, $P < 0.05$; Fig. 3f). By contrast, t_{crit_obs} was unrelated to minimum leaf conductance g_{min} (Fig. 3g), the RWC at both stomatal closure (θ_0; Fig. 3a) and Ψ_{crit} (θ_{crit}; Fig. 3b), as well as the difference between these variables ($\theta_0 - \theta_{crit}$; Fig 3c). T_{crit_obs}

was also unrelated to D (VPD) during each species' dry-down phase (Fig. 3h).

Variation in t_{crit_obs} across species was strongly correlated with lower water potentials both at stomatal closure g_{s90} ($r^2 = 0.93$, $P < 0.001$; Fig. 4e) and at 50% loss in stem hydraulic conductance (stem P_{50}; $r^2 = 90$, $P < 0.001$; Fig. 4a). The t_{crit_obs} was positively correlated with stronger hydraulic vulnerability segmentation (i.e. larger differences between leaf and stem P_{50}; $r^2 = 0.89$, $P < 0.001$; Fig. 4c), wider stomatal-hydraulic safety margins (SHSMs; $r^2 = 0.81$, $P = 0.002$; Fig. 4f), and higher plant basal stem area to maximum leaf area (i.e. the Huber value; $r^2 = 0.72$, $P < 0.01$; Fig. 4h). Plant desiccation time was not significantly correlated with shoot capacitance, although there was a trend of shorter t_{crit_obs} in species with higher capacitance (Fig. 4g).

Observed plant dry-down times were positively correlated with the mean aridity (AI; $r^2 = 0.71$, $P = 0.008$) and negatively correlated with the MAP ($r^2 = 0.69$, $P = 0.01$) measured across each species' distribution, but were unrelated to the mean annual temperature (Fig. S6).

Discussion

Our findings suggest the model fitted with a leaf shedding function accurately predicts the time it takes for plants to dehydrate during the final phase of drought, from the point of stomatal closure to critical levels of hydraulic dysfunction (Fig. 2c). Furthermore, strong association between observed and predicted plant desiccation times with t_{crit} calculated using branch-level traits (t_{crit_shoot}) suggests the model could be used to develop an index of plant susceptibility to desiccation across species globally. Although our use of stem P_{88} as a measure of the critical water potential most likely underestimated the point of mortality in these species (see also Li *et al.*, 2016), we argue that the model can be extended to water potentials closer to specific lethal thresholds, up to the point of complete canopy loss. Scaled-up to mature trees, this information, in conjunction with traits that influence plant water availability in the soil (e.g. rooting depth) and rates of plant water use (transpiration) relative to hydraulic safety, will significantly increase our ability to predict when trees across the landscape will die during extreme drought (also see Martin-StPaul *et al.*, 2017).

Performance of the t_{crit} model

The model, when tested using shoot-level traits and a fixed leaf area (t_{crit_shoot}), tended to underestimate observed plant desiccation time across species (Fig. 2a), especially in semi-arid species. The level of underestimation was reduced when the model included the contribution of roots to plant water content V_w (Fig. 2b). However, much closer alignment between observed and predicted plant desiccation times was achieved when the model incorporated a leaf shedding function t_{crit_shed} (Fig. 2c). Leaf shedding has previously been shown to play an important role in delaying the onset of cavitation in stems during drought by reducing evaporative surface area and thereby rates of plant
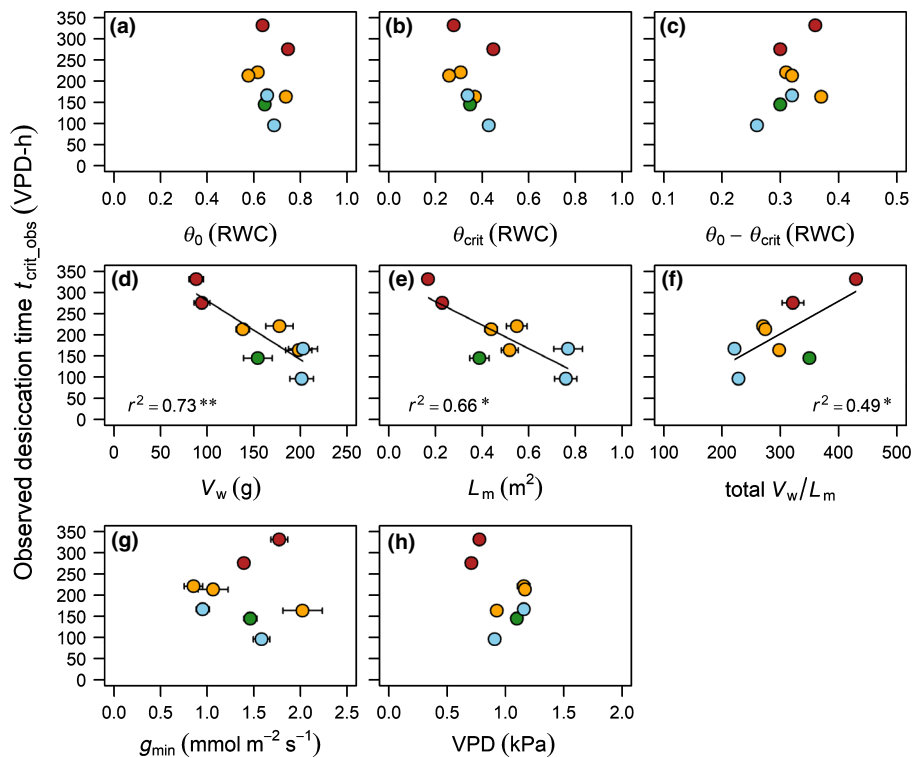
Fig. 3 The relationship (or lack thereof) between different parameters of the t_{crit} model (see Table 2) and observed desiccation time across *Eucalyptus* species. Model parameters include (a) RWC at stomatal closure, θ_0; (b) RWC at Ψ_{crit}, θ_{crit}; (c) the difference between θ_0 and θ_{crit}; (d) total plant water content, V_w; (e) maximum leaf area, L_m; (f) the ratio of V_w to L_m; (g) minimum leaf conductance, gmin; (h) VPD during the desiccation phase. θθcritColours indicate vegetation type: light blue, wet sclerophyll forest; green, dry sclerophyll forest; orange, grassy woodland; red, semi-arid woodland. Error bars are SE. Levels of significance: *, $P \leq 0.05$; **, $P < 0.01$.

water loss (Wolfe *et al.*, 2016; Hochberg *et al.*, 2017). In the current study, the largest increase in plant desiccation time due to leaf shedding was recorded in the arid-zone species *E. largiflorens*, which started to shed leaves at higher water potentials relative to Ψ_{crit} than other species. It is also consistent with large differences between the hydraulic vulnerability of leaves and stems recorded for this and other arid-zone species in our sample group (Li *et al.*, 2019), suggesting that leaves may act as hydraulic fuses in delaying the onset of cavitation in more carbon-expensive stems (Tyree & Ewers, 1991; Johnson *et al.*, 2016). Interestingly, the onset of leaf shedding tended to occur earlier in species from more mesic environments with lower levels of leaf and stem cavitation resistance (Li *et al.*, 2018a, 2019). This suggests a possible causal link between embolism and leaf shedding (Hochberg *et al.*, 2017), although there is still some uncertainty regarding the consistency of the shedding response with leaf water status under strongly contrasting conditions. Nevertheless, given that the mechanism of leaf shedding in these plants was purely drought related, the model presents a viable alternative to approaches employed in global models. Land surface models currently represent leaf turnover using simplistic assumptions related to day length, temperature, and/or soil moisture availability (Dahlin *et al.*, 2017). In those models (e.g. Lpj-guess and Orchidee) that do increase the turnover rate of leaves in response to drought, the thresholds used lack an empirical basis and lead to divergent responses across models (De Kauwe *et al.*, 2017).

A major assumption in the t_{crit} model is that plant roots become hydraulically isolated from the soil at the point of stomatal closure (i.e. plant water uptake stops), and that subsequent rates of plant desiccation are independent of rates of soil dry-down. Root hydraulic isolation is thought to minimize plant water loss back into dry soil and has been observed in a number of species, particularly desert succulents (North & Nobel, 1992) and desiccation-avoidance saplings (Plaut *et al.*, 2013; Wolfe, 2017). Importantly, in a recent study that grew plants in the same loamy-sand soil as used in the current experiment, Drake *et al.* (2017) observed separation between plant and soil water potential at the point of stomatal closure in three woody angiosperms (including two species of eucalypt) and the conifer *Pinus radiata*. Nevertheless, differences in root morphology, as well as differences in soil characteristics, indicate that not all plants are able to disconnect from drying soil, which may result in faster or slower dry-down times to mortality (Wolfe, 2017). In these instances, modelled plant dry-down times to Ψ_{crit} would need to incorporate the additional influence of the soil water-holding capacity, as well as rates of evaporative soil water loss.

Influence of model parameters

The ratio of maximum plant water content to total canopy leaf area $V_w : L_m$ was correlated with t_{crit_obs} across species (Fig. 3), with higher $V_w : L_m$ ratios and longer desiccation times recorded in species from more arid environments. This finding is consistent with a previous study that described high $V_w : L_m$ ratios in terms of their benefit to plants enduring long dry seasons in the tropics (Tyree *et al.*, 1991) and highlights $V_w : L_m$ as an important determinant of species' drought tolerance and mortality risk. Additionally, it is worth noting that the strength of the contribution of $V_w : A_L$ to both predicted and observed plant desiccation time should increase with increasing plant size, where stem volume, and thus water content, generally increases relative to canopy area (Scholz *et al.*, 2011).
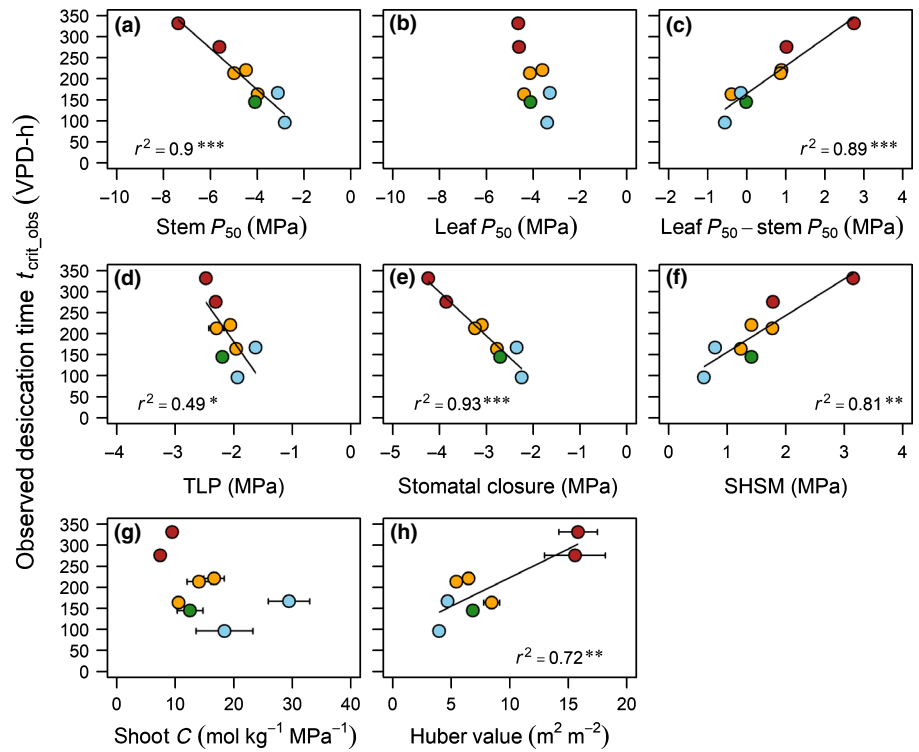
Fig. 4 Relationships across *Eucalyptus* species between commonly measured hydraulic traits (see Supporting Information Table S1 for species values) and t_{crit_obs}. Traits include the hydraulic vulnerability of (a) stems (stem P_{50}) and (b) leaves (leaf P_{50}), (c) vulnerability segmentation (leaf P_{50} − stem P_{50}), (d) turgor loss point (TLP), (e) the water potential at stomatal closure (g_{s90}), (f) the stomatal-hydraulic safety margin (SHSM; stem P_{50} − g_{s90}), (g) shoot capacitance (shoot C), and (h) Huber value. Colours indicate vegetation type: light blue, wet sclerophyll forest; green, dry sclerophyll forest; orange, grassy woodland; red, semi-arid woodland. Error bars are SE. Levels of significance: *, $P \leq 0.05$; **, $P < 0.01$; ***, $P < 0.001$.

Importantly, the model allows for relatively easy scaling to mature trees given the strong allometric relationship between stem volume and leaf area observed across plant sizes for many species (Falster *et al.*, 2015).

By contrast, plant desiccation time was unrelated to the minimum conductance of individual leaves g_{min}. This is consistent with previous work suggesting g_{min} is highly responsive to growth conditions (Duursma *et al.*, 2019), although some studies have shown the adaptive value of low g_{min} with respect to drought tolerance (Burghardt & Riederer, 2003; Brodribb *et al.*, 2014). Plant desiccation time was also unrelated to the RWC at g_{s90} and Ψ_{crit}, and somewhat unexpectedly was unrelated to the span of RWC between these thresholds. Importantly, these findings suggest that knowledge of RWC alone may not be sufficient to differentiate the limits of species tolerance to drought. Nevertheless, and as demonstrated in the current study, there is resurgent focus on RWC as an indicator of plant water status and its role in determining mortality risk during drought, especially when integrated with key drought tolerance traits and thresholds of lethal drought stress (Martinez-Vilalta *et al.*, 2018).

Correlations with hydraulic traits

Across the eight species of eucalypt examined in this study, plant desiccation time was strongly correlated with cavitation resistance. In effect, species with higher cavitation resistance achieved longer desiccation times from g_{s90} to Ψ_{crit}. This result suggests that, in addition to being a key determinant of drought survivorship (Brodribb & Cochard, 2009; Urli *et al.*, 2013), cavitation resistance also influences the timing of hydraulic failure during

extreme drought (Martin-StPaul *et al.*, 2017). Plant desiccation time was also inversely correlated with the water potential at stomatal closure, with longer desiccation times recorded in species with delayed stomatal closure. However, the more meaningful metric for assessing the time to hydraulic failure is the SHSM, which was also shown to be correlated with plant desiccation time here, as well as in previous studies (Martin-StPaul *et al.*, 2017; Blackman *et al.*, 2019). Contrary to expectations, plants with higher capacitance did not achieve longer plant desiccation times. In fact, we observed a trend of increasing desiccation time with decreasing capacitance, which is consistent with previous findings (Gleason *et al.*, 2014) and points to the trade-off between cavitation resistance and capacitance already shown in these species (Li *et al.*, 2018a). Nevertheless, it is reasonable to suggest that capacitance may exert a stronger influence on plant desiccation time, both in mature trees where the contribution of stem-specific hydraulic capacitance may be higher (Scholz *et al.*, 2011) and in species with strong drought-avoidance strategies (Wolfe, 2017; Blackman *et al.*, 2019).

Relevance to trees in the field

It is important to acknowledge that, in the current study, plant desiccation time was measured for all species using plants grown and dried-down under approximately the same VPD conditions. Hence, it is not entirely surprising that both predicted and observed t_{crit} varied in accordance with species ecological niche. If the plants had been dried-down under their respective home-climate conditions, the model output and species ranking of t_{crit} may differ from those reported here. Indeed, when t_{crit} was

calculated for each species using the VPD characteristic of its native distribution, there was no relationship between observed and predicted desiccation time, and the otherwise strong signal of home-site aridity was absent. However, it is important to acknowledge that key traits in the model, such as g_{min} and V_w/L_m, can be highly plastic and would also be expected to differ significantly from those reported here when measured in trees from the field. Thus, in order to predict field-relevant desiccation time for specific species, the model should ultimately be parameterized with traits and VPD conditions derived from the field.

The relevance of t_{crit} also depends on the likelihood of plants in the field being exposed to water stress sufficiently severe to cause stomatal closure. Some drought-avoidant species, for example, are able to maintain transpiration during long periods of drought via deep roots and access to ground water (Nardini *et al.*, 2016). In these cases, the occurrence of stomatal closure and the onset of the final dry-down phase relevant to the model may be rare. Such species may also have low cavitation resistance, which would lead to an overestimation of mortality risk. Thus, in the context of predicting when trees will succumb during drought in the field, desiccation time should ultimately be considered in relation to the environmental and climatic conditions that shape species overall water-use strategy.

Conclusions and future directions

This work demonstrates that the duration of the final phase of drought stress, from stomatal closure to critical levels of hydraulic failure, can be predicted using a relatively simple trait-based model. It supports other models of the time required to observe plant hydraulic failure during drought (Martin-StPaul *et al.*, 2017) and complements models of stomatal behaviour relative to hydraulic safety during early-phase drought (Mackay *et al.*, 2015; Sperry & Love, 2015). In the current study, the t_{crit} model performed best when it included a function for drought-induced leaf shedding. Thus, considering the paucity of information relating to the mechanisms and progression of leaf shedding, as well as its relevance to dynamic land surface models, we recommend quantification of leaf area adjustment in diverse species during drought. It is also important to acknowledge that the current model of t_{crit} is relevant only while plants retain some leaf area to enable water loss via g_{min}. Yet, the point of mortality in some angiosperms, especially drought deciduous species, likely occurs sometime after complete leaf shedding (Li *et al.*, 2016; Wolfe *et al.*, 2016). In these species, dehydration will continue via water loss through the bark, the rate of which is currently unknown in most species. Thus, we recommend future models of plant desiccation time incorporate measurements of bark conductance, which will allow t_{crit} to be calculated through to the point of mortality.

The risk of drought mortality will increase with rising temperatures (Allen *et al.*, 2015), so we recommend assessment of the temperature dependence of traits such as g_{min} (Schuster *et al.*, 2016) and its effect on rates of plant dehydration and hydraulic function during especially hot drought events (Cochard, 2019). Finally, we recommend t_{crit} be examined using phylogenetically diverse species with contrasting water-use strategies, as well as in plants grown under a range of environmental conditions, in order to test the generality of its relevance to drought adaptation.

Author contributions

CJB, RAD, BC, DTT, PDR, and BEM designed the experiment. CJB and XL ran the experiment. CJB and BEM analysed the data. CJB wrote the manuscript and BC, DTT, PDR, MGDK, and BEM revised the manuscript.

ORCID

Chris J. Blackman (iD) https://orcid.org/0000-0002-7057-956X
Brendan Choat (iD) https://orcid.org/0000-0002-9105-640X
Martin G. De Kauwe (iD) https://orcid.org/0000-0002-3399-9098
Remko A. Duursma (iD) https://orcid.org/0000-0002-8499-5580
Ximeng Li (iD) https://orcid.org/0000-0002-7816-5441
Belinda E. Medlyn (iD) https://orcid.org/0000-0001-5728-9827
Paul D. Rymer (iD) https://orcid.org/0000-0003-0988-4351
David T. Tissue (iD) https://orcid.org/0000-0002-8497-2047

References

Adams HD, Zeppel MJB, Anderegg WRL, Hartmann H, Landhausser SM, Tissue DT, Huxman TE, Hudson PJ, Franz TE, Allen CD *et al.* **2017.** A multi-species synthesis of physiological mechanisms in drought-induced tree mortality. *Nature Ecology & Evolution* **1**: 1285–1291.

Allen CD, Breshears DD, McDowell NG. 2015. On underestimation of global vulnerability to tree mortality and forest die-off from hotter drought in the Anthropocene. *Ecosphere* **6**: 1–55.

Anderegg WRL, Flint A, Huang C-y, Flint L, Berry JA, Davis FW, Sperry JS, Field CB. 2015. Tree mortality predicted from drought-induced vascular damage. *Nature Geoscience* **8**: 367–371.

Anderegg WRL, Klein T, Bartlett M, Sack L, Pellegrini AFA, Choat B, Jansen S. 2016. Meta-analysis reveals that hydraulic traits explain cross-species patterns of drought-induced tree mortality across the globe. *Proceedings of the National Academy of Sciences, USA* **113**: 5024–5029.

Bartlett MK, Zhang Y, Kreidler N, Sun SW, Ardy R, Cao KF, Sack L. 2014. Global analysis of plasticity in turgor loss point, a key drought tolerance trait. *Ecology Letters* **17**: 1580–1590.

Blackman CJ, Creek D, Maier C, Aspinwall MJ, Drake JE, Pfautsch S, O'Grady AP, Delzon S, Medlyn BE, Tissue DT *et al.* **2019.** Drought response strategies and hydraulic traits contribute to mechanistic understanding of plant dry-down to hydraulic failure. *Tree Physiology* **39**: 910–924.

Blackman CJ, Pfautsch S, Choat B, Delzon S, Gleason SM, Duursma RA. 2016. Toward an index of desiccation time to tree mortality under drought. *Plant, Cell & Environment* **39**: 2342–2345.

Booth TH, Broadhurst LM, Pinkard E, Prober SM, Dillon SK, Bush D, Pinyopusarerk K, Doran JC, Ivkovich M, Young AG. 2015. Native forests and climate change: lessons from eucalypts. *Forest Ecology and Management* 347: 18–29.

Brodribb TJ. 2009. Xylem hydraulic physiology: the functional backbone of terrestrial plant productivity. *Plant Science* 177: 245–251.

Brodribb TJ, Cochard H. 2009. Hydraulic failure defines the recovery and point of death in water-stressed conifers. *Plant Physiology* 149: 575–584.

Brodribb TJ, McAdam SAM, Jordan GJ, Martins SCV. 2014. Conifer species adapt to low-rainfall climates by following one of two divergent pathways. *Proceedings of the National Academy of Sciences, USA* 111: 14489–14493.

Brodribb TJ, Skelton RP, McAdam SAM, Bienaime D, Lucani CJ, Marmottant P. 2016. Visual quantification of embolism reveals leaf vulnerability to hydraulic failure. *New Phytologist* 209: 1403–1409.

Bucci SJ, Goldstein G, Meinzer FC, Franco AC, Campanello P, Scholz FG. 2005. Mechanisms contributing to seasonal homeostasis of minimum leaf water potential and predawn disequilibrium between soil and plant water potential in neotropical savanna trees. *Trees – Structure and Function* 19: 296–304.

Burghardt M, Riederer M. 2003. Ecophysiological relevance of cuticular transpiration of deciduous and evergreen plants in relation to stomatal closure and leaf water potential. *Journal of Experimental Botany* 54: 1941–1949.

Choat B, Brodribb TJ, Brodersen CR, Duursma RA, Lopez R, Medlyn BE. 2018. Triggers of tree mortality under drought. *Nature* 558: 531–539.

Choat B, Jansen S, Brodribb TJ, Cochard H, Delzon S, Bhaskar R, Bucci SJ, Feild TS, Gleason SM, Hacke UG *et al.* 2012. Global convergence in the vulnerability of forests to drought. *Nature* 491: 752–755.

Cochard H. 2019. A new mechanism for tree mortality due to drought and heatwaves. *bioRxiv*: 531632. doi: 10.1101/531632.

Dahlin KM, Ponte DD, Setlock E, Nagelkirk R. 2017. Global patterns of drought deciduous phenology in semi-arid and savanna-type ecosystems. *Ecography* 40: 314–323.

De Kauwe MG, Medlyn BE, Walker AP, Zaehle S, Asao S, Guenet B, Harper AB, Hickler T, Jain AK, Luo Y. 2017. Challenging terrestrial biosphere models with data from the long-term multifactor Prairie Heating and CO_2 Enrichment experiment. *Global Change Biology* 23: 3623–3645.

Delzon S, Cochard H. 2014. Recent advances in tree hydraulics highlight the ecological significance of the hydraulic safety margin. *New Phytologist* 203: 355–358.

Drake JE, Power SA, Duursma RA, Medlyn BE, Aspinwall MJ, Choat B, Creek D, Eamus D, Maier C, Pfautsch S *et al.* 2017. Stomatal and non-stomatal limitations of photosynthesis for four tree species under drought: a comparison of model formulations. *Agricultural and Forest Meteorology* 247: 454–466.

Duke NC, Kovacs JM, Griffiths AD, Preece L, Hill DJE, van Oosterzee P, Mackenzie J, Morning HS, Burrows D. 2017. Large-scale dieback of mangroves in Australia's Gulf of Carpentaria: a severe ecosystem response, coincidental with an unusually extreme weather event. *Marine and Freshwater Research* 68: 1816–1829.

Duursma RA, Blackman CJ, Lopéz R, Martin-StPaul NK, Cochard H, Medlyn BE. 2019. On the minimum leaf conductance: its role in models of plant water use, and ecological and environmental controls. *New Phytologist* 221: 693–705.

Falster DS, Duursma RA, Ishihara MI, Barneche DR, FitzJohn RG, Vårhammar A, Aiba M, Ando M, Anten N, Aspinwall MJ *et al.* 2015. BAAD: a biomass and allometry database for woody plants. *Ecology* 96: 1445–1445.

Gleason SM, Blackman CJ, Cook AM, Laws CA, Westoby M. 2014. Whole-plant capacitance, embolism resistance and slow transpiration rates all contribute to longer desiccation times in woody angiosperms from arid and wet habitats. *Tree Physiology* 34: 275–284.

Hochberg U, Windt CW, Ponomarenko A, Zhang YJ, Gersony J, Rockwell FE, Holbrook NM. 2017. Stomatal closure, basal leaf embolism, and shedding protect the hydraulic integrity of grape stems. *Plant Physiology* 174: 764–775.

Johnson DM, Wortemann R, McCulloh KA, Jordan-Meille L, Ward E, Warren JM, Palmroth S, Domec JC. 2016. A test of the hydraulic vulnerability segmentation hypothesis in angiosperm and conifer tree species. *Tree Physiology* 36: 983–993.

Kerstiens G. 1996. Cuticular water permeability and its physiological significance. *Journal of Experimental Botany* 47: 1813–1832.

Li S, Feifel M, Karimi Z, Schuldt B, Choat B, Jansen S. 2016. Leaf gas exchange performance and the lethal water potential of five European species during drought. *Tree Physiology* 36: 179–192.

Li XM, Blackman CJ, Choat B, Duursma RA, Rymer PD, Medlyn BE, Tissue DT. 2018a. Tree hydraulic traits are coordinated and strongly linked to climate-of-origin across a rainfall gradient. *Plant, Cell & Environment* 41: 646–660.

Li XM, Blackman CJ, Peters JM, Choat B, Rymer PD, Medlyn BE, Tissue DT. 2019. More than iso/anisohydry: hydroscapes integrate plant water-use and drought tolerance traits in ten eucalypt species from contrasting climates. *Functional Ecology* 33: 1035–1049.

Li XM, Blackman CJ, Rymer PD, Quintans D, Duursma RA, Choat B, Medlyn BE, Tissue DT. 2018b. Xylem embolism measured retrospectively is linked to canopy dieback in natural populations of *Eucalyptus piperita* following drought. *Tree Physiology* 38: 1193–1199.

Mackay DS, Roberts DE, Ewers BE, Sperry JS, McDowell NG, Pockman WT. 2015. Interdependence of chronic hydraulic dysfunction and canopy processes can improve integrated models of tree response to drought. *Water Resources Research* 51: 6156–6176.

Martinez-Vilalta J, Anderegg WR, Sapes G, Sala A. 2018. Greater focus on water pools may improve our ability to understand and anticipate drought-induced mortality in plants. *New Phytologist* 223: 22–32.

Martin-StPaul N, Delzon S, Cochard H. 2017. Plant resistance to drought depends on timely stomatal closure. *Ecology Letters* 20: 1437–1447.

Matusick G, Ruthrof KX, Brouwers NC, Dell B, Hardy GSJ. 2013. Sudden forest canopy collapse corresponding with extreme drought and heat in a Mediterranean-type eucalypt forest in southwestern Australia. *European Journal of Forest Research* 132: 497–510.

Moore GW, Edgar CB, Vogel JG, Washington-Allen RA, March OG, Zehnder R. 2016. Tree mortality from an exceptional drought spanning mesic to semiarid ecoregions. *Ecological Applications* 26: 602–611.

Nardini A, Battistuzzo M, Savi T. 2013. Shoot desiccation and hydraulic failure in temperate woody angiosperms during an extreme summer drought. *New Phytologist* 200: 322–329.

Nardini A, Casolo V, Dal Borgo A, Savi T, Stenni B, Bertoncin P, Zini L, McDowell NG. 2016. Rooting depth, water relations and non-structural carbohydrate dynamics in three woody angiosperms differentially affected by an extreme summer drought. *Plant, Cell & Environment* 39: 618–627.

Nepstad DC, Tohver IM, Ray D, Moutinho P, Cardinot G. 2007. Mortality of large trees and lianas following experimental drought in an Amazon forest. *Ecology* 88: 2259–2269.

North GB, Nobel PS. 1992. Drought-induced changes in hydraulic conductivity and structure in roots of *Ferocactus acanthodes* and *Opuntia ficus-indica*. *New Phytologist* 120: 9–19.

Pineda-Garcia F, Paz H, Meinzer FC. 2013. Drought resistance in early and late secondary successional species from a tropical dry forest: the interplay between xylem resistance to embolism, sapwood water storage and leaf shedding. *Plant, Cell & Environment* 36: 405–418.

Plaut JA, Wadsworth WD, Pangle R, Yepez EA, McDowell NG, Pockman WT. 2013. Reduced transpiration response to precipitation pulses precedes mortality in a piñon–juniper woodland subject to prolonged drought. *New Phytologist* 200: 375–387.

R Core Team. 2018. *R: A language and environment for statistical computing*. Vienna, Austria: R Foundation for Statistical Computing. [WWW document] URL http://www.R-project.org/.

Resco V, Ewers BE, Sun W, Huxman TE, Weltzin JF, Williams DG. 2009. Drought-induced hydraulic limitations constrain leaf gas exchange recovery after precipitation pulses in the C_3 woody legume, *Prosopis velutina*. *New Phytologist* 181: 672–682.

Salomon RL, Limousin JM, Ourcival JM, Rodriguez-Calcerrada J, Steppe K. 2017. Stem hydraulic capacitance decreases with drought stress: implications for modelling tree hydraulics in the Mediterranean oak *Quercus ilex*. *Plant, Cell & Environment* 40: 1379–1391.

Scholz FG, Phillips N, Bucci SJ, Meinzer FC, Goldstein G. 2011. Hydraulic capacitance: biophysics and functional significance of internal water sources in relation to tree size. In: Meinzer FC, Lachenbruch B, Dawson TE, eds. *Size- and age-related changes in tree structure and function*. Dordrecht, the Netherlands: Springer, 341–361.

Schuster AC, Burghardt M, Alfarhan A, Bueno A, Hedrich R, Leide J, Thomas J, Riederer M. 2016. Effectiveness of cuticular transpiration barriers in a desert plant at controlling water loss at high temperatures. *AoB Plants* 8: plw027.

Schuster AC, Burghardt M, Riederer M. 2017. The ecophysiology of leaf cuticular transpiration: are cuticular water permeabilities adapted to ecological conditions? *Journal of Experimental Botany* 68: 5271–5279.

Skelton RP, West AG, Dawson TE. 2015. Predicting plant vulnerability to drought in biodiverse regions using functional traits. *Proceedings of the National Academy of Sciences, USA* 112: 5744–5749.

Sperry JS, Love DM. 2015. What plant hydraulics can tell us about responses to climate-change droughts. *New Phytologist* 207: 14–27.

Trenberth KE, Dai AG, van der Schrier G, Jones PD, Barichivich J, Briffa KR, Sheffield J. 2014. Global warming and changes in drought. *Nature Climate Change* 4: 17–22.

Tyree MT, Ewers FW. 1991. The hydraulic architecture of trees and other woody-plants. *New Phytologist* 119: 345–360.

Tyree MT, Hammel HT. 1972. Measurement of turgor pressure and water relations of plants by pressure-bomb technique. *Journal of Experimental Botany* 23: 267–282.

Tyree MT, Snyderman DA, Wilmot TR, Machado JL. 1991. Water relations and hydraulic architecture of a tropical tree (*Schefflera morototoni*) – data, models, and a comparison with 2 temperate species (*Acer saccharum* and *Thuja occidentalis*). *Plant Physiology* 96: 1105–1113.

Tyree MT, Sperry JS. 1989. Vulnerability of xylem to cavitation and embolism. *Annual Review of Plant Physiology and Plant Molecular Biology* 40: 19–38.

Tyree MT, Yang SD. 1990. Water-storage capacity of *Thuja*, *Tsuga* and *Acer* stems measured by dehydration isotherms. *Planta* 182: 420–426.

Urli M, Porte AJ, Cochard H, Guengant Y, Burlett R, Delzon S. 2013. Xylem embolism threshold for catastrophic hydraulic failure in angiosperm trees. *Tree Physiology* 33: 672–683.

Venturas MD, MacKinnon ED, Dario HL, Jacobsen AL, Pratt RB, Davis SD. 2016. Chaparral shrub hydraulic traits, size, and life history types relate to species mortality during California's historic drought of 2014. *PLoS ONE* 11: e0159145.

Wolfe BT. 2017. Retention of stored water enables tropical tree saplings to survive extreme drought conditions. *Tree Physiology* 37: 469–480.

Wolfe BT, Sperry JS, Kursar TA. 2016. Does leaf shedding protect stems from cavitation during seasonal droughts? A test of the hydraulic fuse hypothesis. *New Phytologist* 212: 1007–1018.

Supporting Information

Additional Supporting Information may be found online in the Supporting Information section at the end of the article.

Fig. S1 Shoot capacitance curves.

Fig. S2 Leaf shedding response function.

Fig. S3 Relative water content and water potential in shoots and leaves.

Fig. S4 Leaf shedding in response to decreasing water potential.

Fig. S5 t_{crit} vs t_{crit_obs}, with the model using each species home-climate VPD.

Fig. S6 The relationship between t_{crit_obs} and species home-climate.

Notes S1 Extending the t_{crit} desiccation time model to include leaf shedding.

Table S1 Summary of species hydraulic trait means.

Table S2 Model output for leaf shedding function with species pooled by vegetation type.

Please note: Wiley Blackwell are not responsible for the content or functionality of any Supporting Information supplied by the authors. Any queries (other than missing material) should be directed to the *New Phytologist* Central Office.